European Journal of Medicinal Chemistry 75 (2014) 11–20

Contents lists available at ScienceDirect

European Journal of Medicinal Chemistry

journal homepage: http://www.elsevier.com/locate/ejmech

Original article

# Integrating docking scores, interaction profiles and molecular descriptors to improve the accuracy of molecular docking: Toward the discovery of novel Akt1 inhibitors

Wenhu Zhan [a], Daqiang Li [a], Jinxin Che [a], Liangren Zhang [b], Bo Yang [c], Yongzhou Hu [a], Tao Liu [a,**], Xiaowu Dong [a,*]

[a] ZJU-ENS Joint Laboratory of Medicinal Chemistry, Zhejiang Province Key Laboratory of Anti-Cancer Drug Research, College of Pharmaceutical Sciences, Zhejiang University, Hangzhou 310058, China
[b] State Key Laboratory of Natural and Biomimetic Drugs, Peking University, Beijing 100083, China
[c] Department of Pharmacology, School of Medicine, Zhejiang University, Hangzhou 310058, China

ARTICLE INFO

*Article history:*
Received 4 September 2013
Received in revised form
8 January 2014
Accepted 13 January 2014
Available online 22 January 2014

*Keywords:*
Akt1 inhibitors
Molecular docking
Support vector regression (SVR)
Synthesis
Antiproliferative activity

ABSTRACT

A set of forty-seven Akt1 inhibitors was used for the development of molecular docking based QSAR model by using nonlinear regression. The integration of docking scores, key interaction profiles and molecular descriptors remarkably improved the accuracy of the QSAR models, providing reasonable statistical parameters ($R^2_{train}$ = 0.948, $R^2_{test}$ = 0.907 and $Q^2_{cv}$ = 0.794). The established **MD-SVR** model based structural modification of new 4-amino-pyrimidine derivatives was further performed, and six compounds **56a**,**b** and **60a**–**d** with good prediction activities were synthesized and biologically evaluated. All of these compounds exhibited promising Akt1 inhibitory and antiproliferative activities, suggesting the reliability and good application value of the established **MD-SVR** model in the development of Akt1 inhibitors.



## 1. Introduction

Structure-based drug design (SBDD) is a rational strategy for identification of bioactive hits and optimization of lead compounds. Several tools are commonly used in SBDD, such as molecular docking, NMR spectroscopy and X-ray crystallography. Molecular docking is a computational technique that can rapidly propose a binding mode between a ligand and its receptor. The reliability of molecular docking in SBDD is significantly affected by the accuracy of docking scores and the 3D-structure of receptor. Recently, there is a growing interest in applying mathematical methods to improve the accuracy of molecular docking, including multiple linear regression (MLR), artificial neural network (ANN) and support vector machine (SVM). Among them, SVM is a popular algorithm developed from the machine learning community [1], showing good predictive ability in QSAR studies [2,3]. For example, Chen et al., demonstrated that seven docking scores were integrated by the support vector rank regression (SVRR) algorithm to improve the prediction for binding conformation [4]. In addition, the accuracy of molecular docking can be improved by integrating additional variables that indicate the fitness of a computed binding conformation [5–7].

The serine/threonine kinase Akt (also known as protein kinase B) has become a promising potential target because of its essential regulatory role in cellular processes, including cancer progression and insulin metabolism [8–12]. Akt regulates cell growth through its effects on the TSC1/TSC2 complex and mTOR pathways, as well as cell cycle and cell proliferation [13–15]. Inhibition of Akt activities can result in increasing apoptosis of cancer cells, and decreasing tumor growth [11,16–18]. Currently, many companies and academic laboratories have initiated a variety of approaches to inhibit the Akt pathway [16,19–21], leading to the discovery of a number of Akt inhibitors. However, there are still some issues (e.g. selectivity, toxicity and efficacy) that need to be resolved. Thus, it is still greatly of interest in the development of novel Akt inhibitors, especially for reliable and efficient method to accelerate the process. According to the presence of high resolution 3D structures of

* Corresponding author. Tel./fax: +86 571 88981051.
** Corresponding author. Tel./fax: +86 571 88208460.
*E-mail addresses:* lt601@zju.edu.cn (T. Liu), dongxw@zju.edu.cn (X. Dong).

0223-5234/$ – see front matter © 2014 Elsevier Masson SAS. All rights reserved.
http://dx.doi.org/10.1016/j.ejmech.2014.01.019

Akt1 bound with its inhibitors, structure-based drug design would be a promising strategy.

Although several attempts have been made recently in generating the predictive models for Akt1 inhibitors through ligand-based methods [22,23], there is few structure-based predictive QSAR models for identification and optimization of Akt1 inhibitors. Herein, molecular docking based support vector regression (**MD-SVR**) method was applied to establish a reliable structure-based QSAR model. As revealed both in X-ray diffraction and molecular docking of ligand-bound Akt1 complex, several crucial interactions were commonly observed, such as amino acid residues Glu228, Ala230, Glu234, Glu292 and Phe163. In addition, considering that hydrophilic and hydrophobic interactions are two major intermolecular forces, molecular descriptors (e.g. ClogP and tPSA) would be important properties for binding affinity of the ligands with Akt1. Thus, in addition to the generated docking scores by molecular docking, key interactions profiles and molecular descriptors (Supporting information, Table S1) were integrated, with aim to enhance the accuracy and reliability of molecular docking (Scheme 1).

The robustness of the established **MD-SVR** model was validated by the prediction for training and test set, as well as the internal leave-one-out cross validation. Moreover, the **MD-SVR** model was used in structure-based design of 4-aminopyrimidine derivatives as novel Akt1 inhibitors. Six compounds with good prediction Akt1 inhibitory activities were synthesized and biological evaluated for Akt1 inhibitory and antiproliferative activities against cancer cell lines.

## 2. Computational method

### 2.1. Data set

For molecular docking based QSAR modeling, a set of forty-seven molecules (Fig. 1) were selected from the literature [18,24–27]. Akt1 inhibitory activity data (Table 1) of them span over 4 orders of magnitude (from 2 to 4000 nM). The biological data of Akt1 inhibitory activities [$IC_{50}$ (nM)] were converted to logarithmic scale [$-$Log $IC_{50}$] and then used for subsequent QSAR analyses as the response variable (dependent variable). For model training and validation, the total data set ($n = 47$) was randomly divided into training set ($n = 36$) and test set ($n = 11$). The 3D-strucure of all compounds were generated and optimized in Discovery Studio 2.0 software (Accelrys, Inc. San Diego, CA) using the CHARMm-like force field [28].

### 2.2. Molecular docking with LigandFit [29]

The docking pocket of Akt1 (PDB ID: 3OCB) was obtained using the LigandFit site search utility in Discovery studio 2.5. For the generation of ligands' conformations, variable numbers of Monte Carlo simulations were used. All the calculations were performed under the PLP Force Field formalism [30]. A short rigid body minimization was then performed, and 50 poses for each ligand were saved for further analysis. Scoring was performed with a set of scoring functions (i.e. Dock_score, LigScore2, PLP1, Jain and PMF) implemented in LigandFit module. The combination of consensus scoring method and the interaction mode analysis was applied to select the preferable output conformation.

### 2.3. Support vector regression (SVR) method [1]

The basic idea of SVM regression is to map the data $x$ into a higher-dimensional feature space $F$ via a nonlinear mapping $\Phi$ and then to do linear regression in this space. Therefore, regression approximation addresses the problem of estimating a function based on a given data set $G = \{(x_i, d_i)\}_i^n$ ($x_i$ is the input vector, $d_i$ is the desired value, and $n$ is the total number of data patterns). SVM regression approximates the function in the following form:

$$y = \sum_{i=1}^{l} w_i \phi(x_i) + b \tag{1}$$

where $\phi(x)$ is the high dimensional feature space, which is nonlinearly mapped from the input space $x$ and $w_i$ and $b$ are coefficients. They are estimated by minimizing the regularized risk function $R(C)$

$$R(C) = C\frac{1}{N}\sum_{i=1}^{N} L_{\xi}(d_i, y_i) + \frac{1}{2}\|w\|^2, \tag{2}$$

where

$$L_{\varepsilon}(d_i, y_i) = \begin{cases} |d-y| - \varepsilon & \text{for} |d-y| - \varepsilon \geq 0 \\ 0 & \text{otherwise} \end{cases}, \tag{3}$$

The first term $C\frac{1}{N}\sum_{i=1}^{N} L_{\xi}(d_i, y_i)$ is the so-called empirical error (risk), which is measured by the $\varepsilon$-insensitive loss function (3). The second term $\frac{1}{2}\|w\|^2$, on the other hand, is called the regularized term. $\varepsilon$ is called the tube size of SVM, and $C$ is the regularization

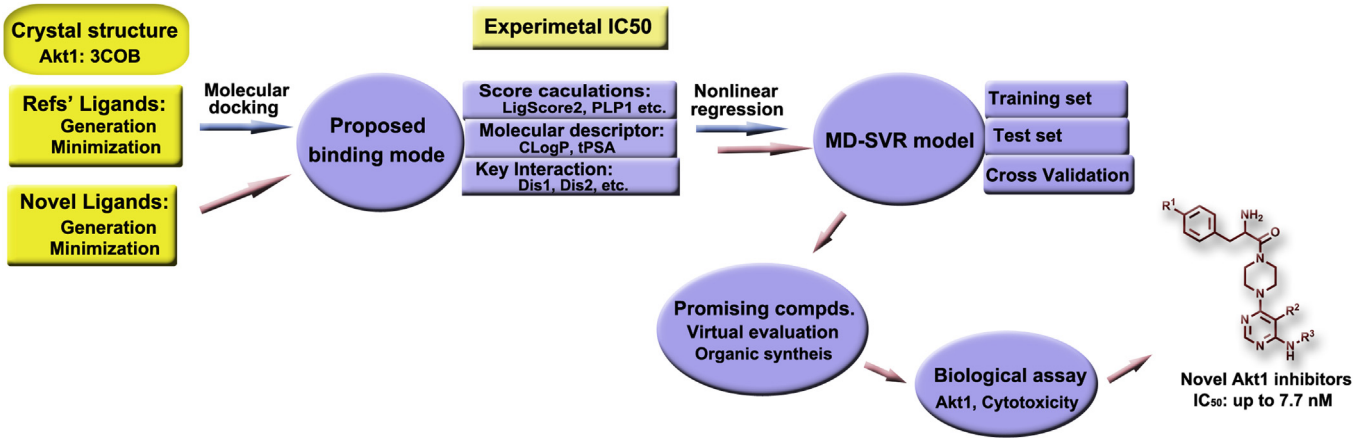


**Scheme 1.** The evolution of the establishment of **MD-SVR** model and its application in development of novel 4-aminopyrimidine derivatives as Akt inhibitors.

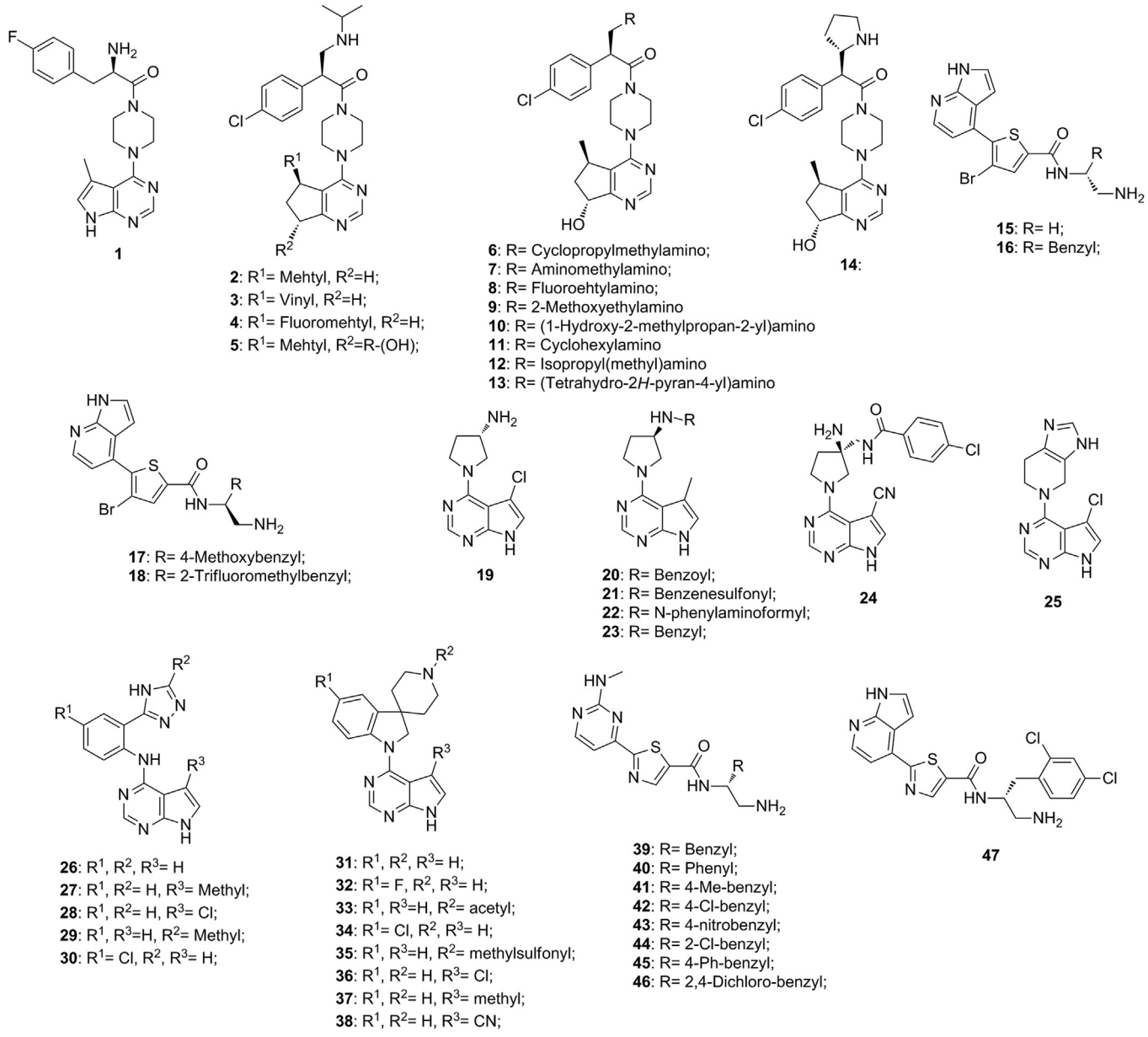


**Fig. 1.** The 2D structures of 47 Akt1 inhibitors used to generate the **MD-SVR** model.

constant determining the trade-off between the empirical error and the regularized term. Introduction of slack variables '$\xi$' leads Eq. (2) to the following constrained function:

$$\text{Minimize } R\left(w,\xi_i,\xi^*\right) = \frac{1}{2}\|w\|^2 + C\sum_{i=1}^{n}\left(\xi_i+\xi_i^*\right), \tag{4}$$

Thus, decision function of Eq. (1) changes to the following form:

$$f\left(x,\alpha_i,\alpha_i^*\right) = \sum_{i=1}^{l}\left(\alpha_i-\alpha_i^*\right)K(x,x_i)+b, \tag{5}$$

where $\alpha_i$ and$\alpha_i^*$ are the introduced Lagrange multipliers and $K(x, x_i)$ is the kernel function. The value is equal to the inner product of two vectors $x$ and $x_i$ in the feature space $\Phi(x)$ and $\Phi(x_i)$, that is, $K(x, x_i) = \Phi(x)^{\mathrm{T}}\Phi(x_i)$. And the radial basis function (RBF) kernel $K(\overline{x_i},\overline{x_j}) = \exp(-\gamma\left\|\overline{x_i}-\overline{x_j}\right\|^2)$ is commonly used.

### 2.4. Leave-one-out cross validation

The leave-one-out cross validation was employed to find the promising QSAR model. Given $n$ samples available in a data set and $m$ candidate models, each model is trained with $n-1$ samples and then is tested on the sample that was left out. This process is repeated $n$ times until every sample in the data set have been used once as a cross-validation instance. Finally, cross validation correlation coefficient ($Q^2_{\mathrm{loo}}$), a measure of the model generalization capability, for all candidate models can be obtained as below:

$$Q^2 = 1-\frac{\sum_{i=1}^{n}(yi-\widehat{yi})^2}{\sum_{i=1}^{n}(yi-ym)^2}$$

where $y_i$ is the desired output, $\widehat{yi}$ is the predicted value by model and $y_m$ is the mean value of dependent variable.

**Table 1**
Compounds **1**–**47** in training set and test set for **MD-SVR** model, and their corresponding experimental and estimated Akt1 inhibitory activities.

| NO. | Experimental | | Predictive | Res. |
|---|---|---|---|---|
| | $IC_{50}$(nM) | $-Log\ IC_{50}$ | $-Log\ IC_{50}$[b] | |
| **1** | 3 | 8.52 | 8.25 | 0.27 |
| **2** | 6 | 8.22 | 8.20 | 0.02 |
| **3** | 2 | 8.70 | 8.18 | 0.52 |
| **4** | 3 | 8.52 | 8.25 | 0.27 |
| **5** | 5 | 8.30 | 8.27 | 0.03 |
| **6**[a] | 5 | 8.30 | 8.18 | 0.12 |
| **7** | 24 | 7.62 | 7.92 | −0.3 |
| **8** | 12 | 7.92 | 8.09 | −0.17 |
| **9**[a] | 8 | 8.10 | 8.24 | −0.14 |
| **10** | 2 | 8.70 | 8.08 | 0.62 |
| **11** | 9 | 8.05 | 8.25 | −0.2 |
| **12** | 18 | 7.74 | 8.02 | −0.28 |
| **13** | 5 | 8.30 | 8.17 | 0.13 |
| **14** | 3 | 8.52 | 8.31 | 0.21 |
| **15**[a] | 158 | 6.80 | 6.11 | 0.69 |
| **16** | 32 | 7.49 | 7.32 | 0.17 |
| **17** | 3 | 8.52 | 8.24 | 0.28 |
| **18** | 3 | 8.52 | 7.75 | 0.77 |
| **19** | 240 | 6.62 | 6.69 | −0.07 |
| **20**[a] | 700 | 6.15 | 6.21 | −0.06 |
| **21** | 600 | 6.22 | 6.32 | −0.1 |
| **22** | 700 | 6.15 | 6.25 | −0.1 |
| **23** | 2400 | 5.62 | 5.77 | −0.15 |
| **24** | 17.5 | 7.76 | 7.55 | 0.21 |
| **25** | 42 | 7.38 | 7.13 | 0.27 |
| **26**[a] | 210 | 6.68 | 6.70 | 0.62 |
| **27** | 425 | 6.37 | 6.48 | −0.2 |
| **28**[a] | 318 | 6.50 | 6.74 | −0.28 |
| **29** | 151 | 6.82 | 6.90 | 0.21 |
| **30** | 171 | 6.77 | 6.92 | 0.13 |
| **31**[a] | 5.3 | 8.28 | 8.30 | 0.02 |
| **32** | 3.1 | 8.51 | 8.30 | 0.12 |
| **33** | 2790 | 5.55 | 5.65 | 0.52 |
| **34**[a] | 4.8 | 8.32 | 8.32 | 0.03 |
| **35** | 3190 | 5.50 | 5.80 | 0.27 |
| **36** | 5.8 | 8.24 | 8.47 | −0.3 |
| **37**[a] | 4.8 | 8.32 | 8.50 | −0.17 |
| **38** | 2.4 | 8.62 | 8.53 | −0.14 |
| **39** | 180 | 6.74 | 6.91 | 0.69 |
| **40**[a] | 550 | 6.26 | 6.36 | 0.17 |
| **41** | 580 | 6.24 | 6.72 | 0.28 |
| **42** | 150 | 6.82 | 6.62 | 0.77 |
| **43** | 740 | 6.13 | 6.32 | 0.21 |
| **44**[a] | 33 | 7.48 | 6.92 | −0.07 |
| **45** | 4000 | 5.40 | 5.47 | −0.06 |
| **46** | 150 | 6.82 | 6.82 | −0.1 |
| **47** | 25 | 7.60 | 7.38 | −0.1 |

[a] The compounds were used as test set.
[b] The $-Log\ IC_{50}$ was predicted by **MD-SVR** model.

## 3. Results and discussion

### 3.1. The development of *MD-SVR* model

The main objective of this work is to generate structure-based quantitative models using a consensus of molecular docking scores, key interactions profiles and molecular descriptors. Firstly, the docking protocols have been validated by reproducing the bound natural substrate conformation (PDB ID: 3OCB). The RMSD value of proposed ligand from the reference coordinates is 0.24, indicating the good accuracy and reliability of LigandFit program in molecular docking of Akt1. Then, known Akt1 inhibitors **1**–**47** were docked into ATP-bound pocket of Akt1 by LigandFit. A set of scoring functions (i.e. Dock_score, LigScore2, PLP1, Jain and PMF) were calculated (Supporting information, Table S2). Correlating docking scores with Akt1 inhibitory activities was initially performed. Feeble robustness of scoring functions toward prediction was observed (Fig. 2) and their $R^2$ values with respect to activity were <0.417 (for overall set). Hence, these individual scoring functions were not enough accurate to prediction the Akt1 inhibitory activities, prompting us to develop the consensus models that integrating docking scores, the key interactions profiles and molecular descriptors to improve the accuracy. The distance between the key amino acid residue (e.g. Glu228, Ala230, Glu234, Glu292 and Phe163) of Akt1 and docked compounds was recorded as key interactions profiles. Further, molecular descriptors (e.g. ClogP and tPSA) were also used to get better insight into the physicochemical requirements for effective binding of ligands with Akt1.

In **MD-SVR** modeling, the RBF kernel was used as kernel function. Capacity parameter $C$, $\varepsilon$ of $\varepsilon$-insensitive loss function and the corresponding parameters $\gamma$ of RBF kernel need to be optimized. The optimal parameters are found by grid search (GS) method. Parameter $lg2C$, $lg2\gamma$ and $lg2\varepsilon$ was extensively investigated between −10 and 10 with 1 as the increment. The result of this grid search is an error-surface spanned by the model parameters. In order to find the optimized combination of the parameters $C$, $\varepsilon$, and $\gamma$, a process of leave-one-out (LOO) cross validation of training set was performed as shown in Fig. 3. The best choices for $C$, $\varepsilon$ and $\gamma$, are 2, 0.11 and 0.6, respectively, and the corresponding support vector number is 18. The regression model developed was found to be reliable statistically ($R^2_{train} = 0.948$, $R^2_{test} = 0.907$, $R^2_{overall} = 0.934$, $R^2_{cv} = 0.794$) (Fig. 2F). Accordingly, the predicted Akt1 inhibitory activities $-Log\ IC_{50}$ are listed in Table 1.

For example, both of compounds **17** and **45** were docked into ATP-bound pocket of Akt1 using LigandFit program, and the binding modes of them were proposed as shown in Fig. 4. Two hydrogen bonds are formed between 1H-pyrrolo[2,3-b]pyridine moiety of **17** (or aminopyrimidine moiety of **45**) and Glu228 and Ala230 of Akt1. The hydrophobic interaction was observed between 4- methoxyphenyl ring of **17** (or biphenyl ring of **45**) and Phe161 of Akt1. An ionic interaction was observed between primary amino group of **17** and Glu292 of Akt1, while no ionic interaction was observed. For quantitative analysis, the distances of the key interactions mentioned above are recorded (Supporting information, Table S2). As shown in Table 1, the superiority of docking scores (Dock_scores, ligscores2, PMF, PLP1 and Jain) of **17** to that of **45** are not very obvious, although **17** ($-LogIC_{50} = 8.52$) exhibited remarkably more potent than **45** ($-LogIC_{50} = 5.40$). Insight into the binding mode of **17** and **45** to Akt1, accordingly, **17** showed additional ionic interaction with Glu292 when comparing with that of **45**, may due to the much more bulky effect of biphenyl moiety of **45**. Considering the different profiles in key interaction analyses, together with five docking scores and tow molecular descriptors, **MD-SVR** model can accurately predict the potency of compounds **17** and **45**, the deviation for **17** and **45** are 0.28 and −0.06 respectively.

### 3.2. The prediction ability of *MD-SVR* model in design of novel Akt1 inhibitors

The aim of any QSAR modeling is that the developed model should be strong enough to be capable of making accurate and reliable predictions of biological activities of new compounds. Hence, to examine predictive ability of the **MD-SVR** model, a set of novel 4-aminopyrimidine derivatives **56a**,**b** and **60a**–**d** were designed and virtually evaluated by **MD-SVR** model. Firstly, compounds **56a**,**b** and **60a**–**d** were docked into ATP-bound pocket of Akt1 using LigandFit program. Then, the five docking scores, key interaction profiles and molecular descriptors were recorded (Supporting information, Table S2). Based on **MD-SVR** model, the predictive Akt1 inhibitory activities $-Log(IC_{50})$ of these compounds were calculated and presented in Table 1. All of them showed good prediction activities, especially for **60b** and **60c**, the $-Log(IC_{50})$

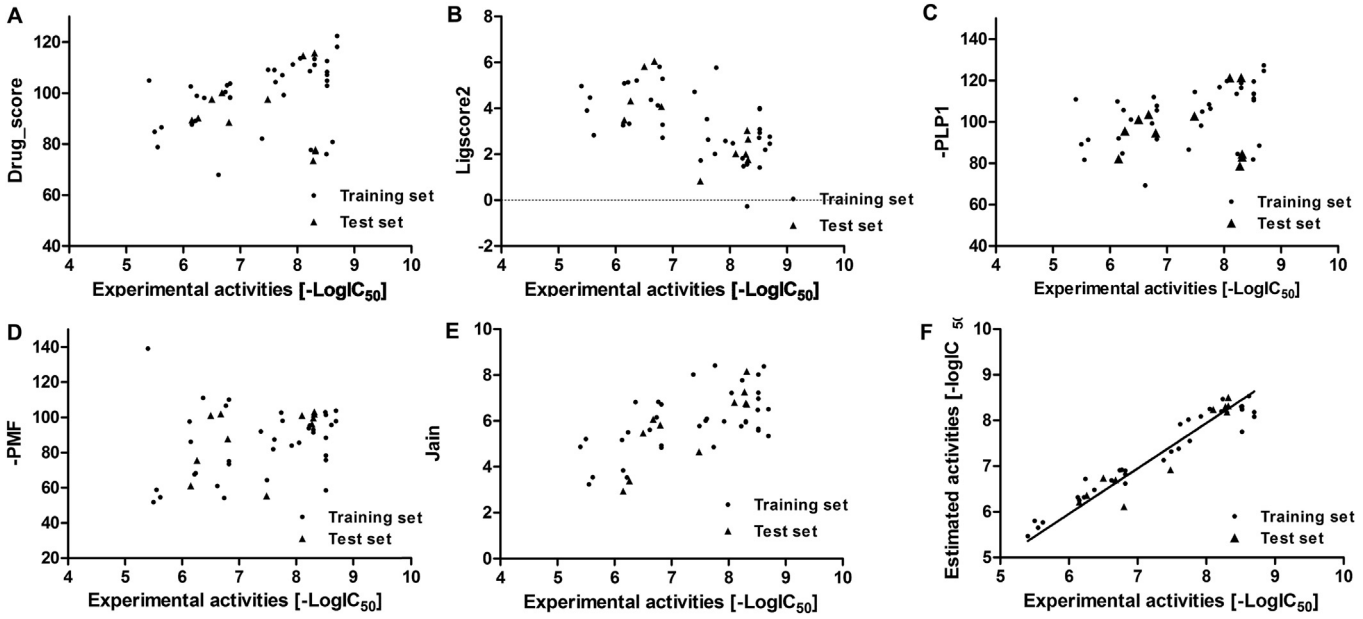


**Fig. 2.** (A) Docking_score vs. experimental Akt inhibitory activities (−Log $IC_{50}$); (B) Ligscore2 vs. experimental Akt inhibitory activities (−Log $IC_{50}$); (C) −PLP vs. experimental Akt inhibitory activities (−Log $IC_{50}$); (D) −PMF vs. experimental Akt inhibitory activities (−Log $IC_{50}$); (E) Jain vs. experimental Akt inhibitory activities (−Log $IC_{50}$); (F) Estimated vs. experimental Akt inhibitory activities (−Log $IC_{50}$) of the **MD-SVR** model.

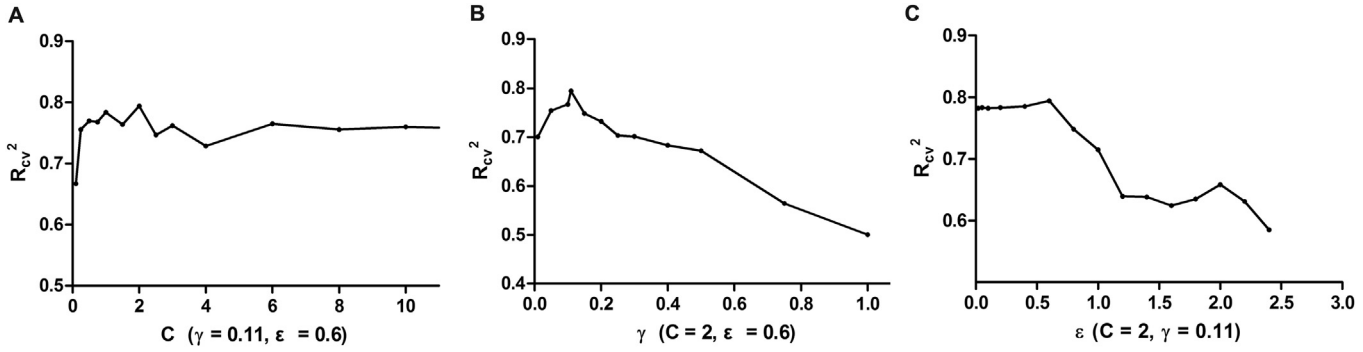


**Fig. 3.** Selection of $\gamma$, $C$ and $\varepsilon$ for training set data in **MD-SVR** model development. (A) $C$ vs.$R^2_{cv}$ on LOO cross-validation. (B) $\gamma$ vs.$R^2_{cv}$ on LOO cross validation. (C) $\varepsilon$ vs.$R^2_{cv}$ on LOO cross validation.

value of which are 7.88 and 7.93, respectively. As exemplified by compound **60c**, the most promising one, the interaction mode of **60c** to Akt1 are similar to that of **17**. As shown in Fig. 5, two hydrogen bonds are formed between 4-aminopyrimidine moiety of **60c** and Glu228 and Ala230 of Akt1. The hydrophobic interaction was observed between 4-chlorophenyl ring of **60c** and Phe161 of Akt1. An additional ionic interaction was observed between primary amino group of **60c** and Glu292 of Akt1.

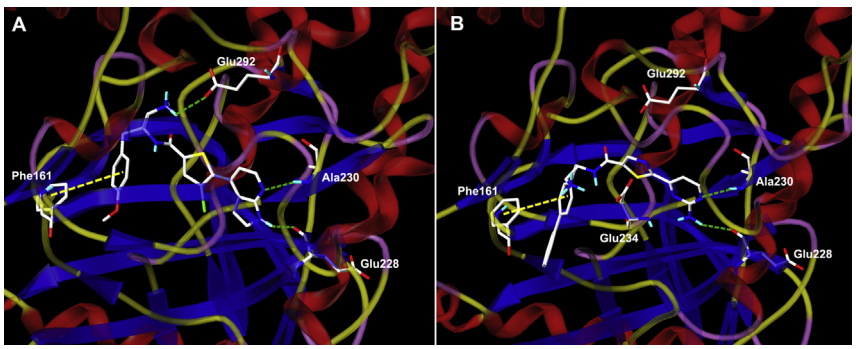


**Fig. 4.** Interaction modes of **17** and **45** to Akt1 proposed by molecular docking. (A) Interaction mode between Akt1 and compound **17**; (B) Interaction mode between Akt1 and compound **45**. Hydrogen bonds and ionic interactions were highlighted by dash green line and the hydrophobic interactions were highlighted by dash yellow line. (For interpretation of the references to color in this figure legend, the reader is referred to the web version of this article.)

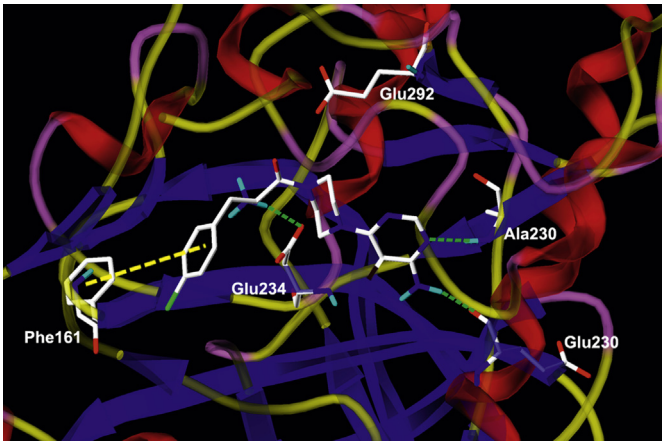


**Fig. 5.** Interaction mode between Akt1 and **60c** proposed by molecular docking. Hydrogen bonds and ionic interactions were highlighted by dash green line and the hydrophobic interactions were highlighted by dash yellow line. (For interpretation of the references to color in this figure legend, the reader is referred to the web version of this article.)

### 3.3. The synthesis of 4-aminopyrimidine derivatives *56a,b* and *60a–d*

The synthesis of 4-aminopyrimidine derivatives **56a**,**b** and **60a**–**d** is outlined in Scheme 2. On one hand, treatment of **48** with benzyl bromide in the presence of $K_2CO_3$ in acetonitrile and subsequent chlorinated with $SOCl_2$ gave the N-protected bis(2-chloroethyl) amine **50** as hydrochloride salt. Compound **51** was obtained by double alkylation of 3,4-dichlorophenylacetonitrile with **50** under basic, phase-transfer conditions. Debenzylation of **51** under mild condition furnished the intermediate **52** in excellent yield. Treatment of 4,6-dichloropyrimidine **53** with either ethanolic methylamine (or aqueous ammonia) afforded 4-amino-6-chloropyrimidines **54**. Treatment of compound **54** with **52** in the presence of $K_2CO_3$ in DMF provides the corresponding **55**. Then, target compound **56** was obtained by reduction of the nitrile group of **55** in the presence of $LiAlH_4$ and $AlCl_3$ in THF.

On the other hand, The N-boc-piperazine and 4-amino-6-chloropyrimidines **54b** were condensed to give **57** in presence of N,N-Diisopropylethylamine (DIPEA) in *n*-BuOH. Treatment of compound **57** with NCS (or NBS) in $CH_2Cl_2$ gave **58**. Deprotection of N-Boc of **58** in acid condition was performed to give key intermediates **59**. Finally, the preparation of the desired compound **60** was achieved by amide coupling, followed by N-Boc deprotection under acidic condition.

### 3.4. Pharmacological assay

Akt1 inhibitory activities of 5**6a**,**b** and **60a**–**d** were determined using a competitive fluorescence polarization kinase activity assay. Compound **H-89** was used as positive control, the determined $IC_{50}$ value of which is consistent with that of literature [31]. Table 2 presents the pharmacological assay results of **56a**,**b** and **60a**–**d**. All of them showed moderate to good Akt1 inhibitory activities. Especially, compounds **60b** and **60c** showed the best Akt1 inhibitory activities ($IC_{50}$ of **60b** and **60c** were 17 nM and 7.7 nM). Comparing with Akt1 inhibitory activities of 5**6a**,**b**, the methylation on 4-amino group of pyrimidine ring didn't affect the Akt1

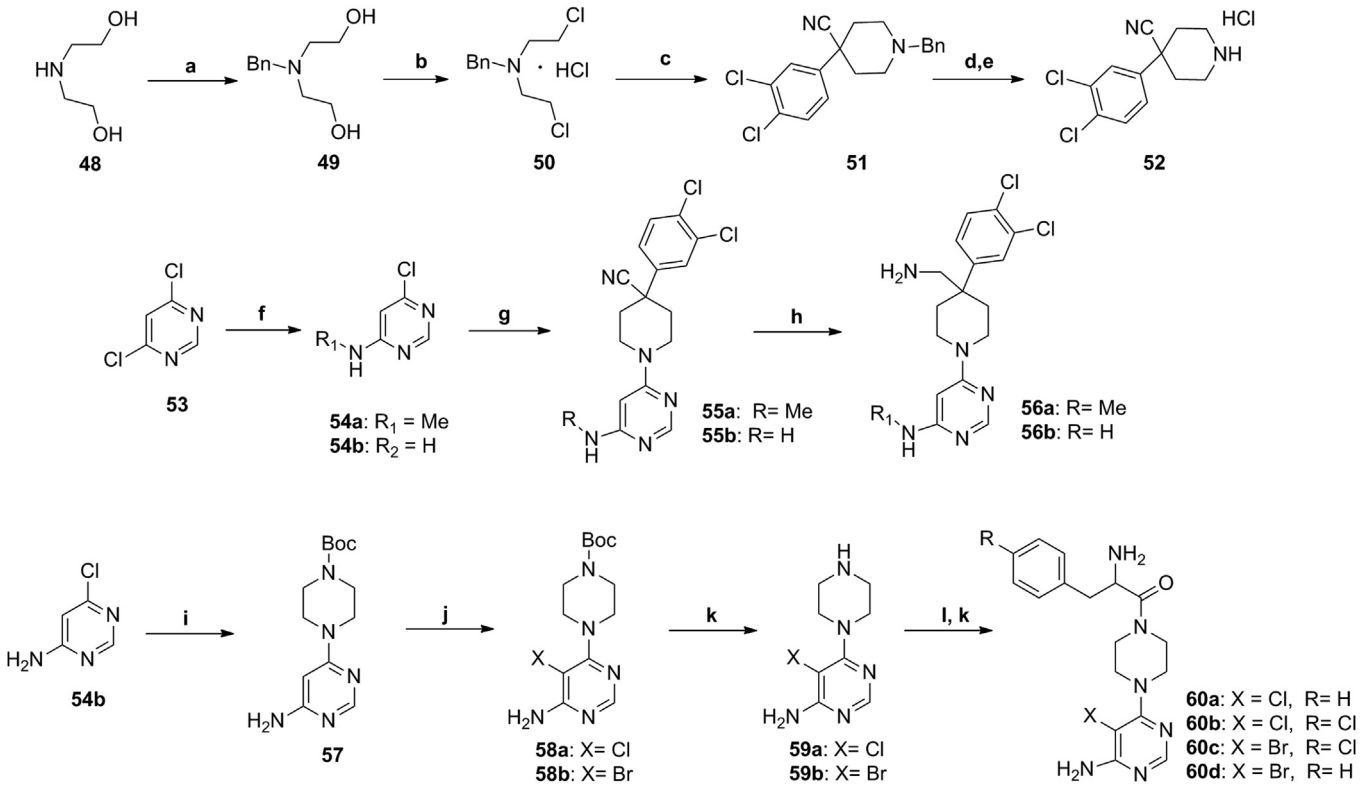


**Scheme 2.** The synthetic route for compounds 5**6a**,**b** and **60a**–**d**. Reaction conditions: a) Benzyl chloride, $K_2CO_3$, $CH_3CN$; b) $SOCl_2$, DCM; c) 2-(3,4-dichlorophenyl)acetonitrile, tetrabutylammonium hydrogen sulfate, 50% NaOH (aq.); d) 2-chloropropanoyl chloride, DCE; e) MeOH, reflux; f) appropriate amine, *i*-PrOH; g) **52**, DMF; h) $LiAlH_4$, $AlCl_3$, THF; i) N-Boc-piperazine, DIPEA, *n*-BuOH; j) NBS or NCS, THF; k) TFA, DCM; l) appropriate N-Boc phenylalanine, EDCl, HOBt, DIPEA, DCM.

**Table 2**
The predictive and experimental Akt1 inhibitory and antiproliferative activities of compounds **56a**,**b** and **60a**–**d**.

| Compd. | Experimental | | Predictive | Antiproliferative activities (μM) | |
|---|---|---|---|---|---|
| | $IC_{50}$(μM) | $-Log(IC_{50})$ | $-Log(IC_{50})$ | OVCAR-8 | HCT116 |
| **56a** | 1.83 | 5.70 | 6.85 | N.T.[a] | 16.70 |
| **56b** | 4.32 | 5.36 | 7.18 | N.T.[a] | 19.84 |
| **60a** | 1.83 | 5.74 | 7.59 | N.T.[a] | 28.69 |
| **60b** | 0.017 | 7.77 | 7.88 | 26.07 | 4.36 |
| **60c** | 0.0077 | 8.11 | 7.93 | 22.67 | 5.15 |
| **60d** | 0.432 | 6.36 | 7.85 | N.T.[a] | 6.19 |
| **H-89** | 2.2 | / | / | 10.50 | 15.70 |

[a] N.T. means no test.

inhibitory activities significantly. Insight into the observed substituent's effects on **60a**–**d** revealed that the chlorine phenyl is essential for Akt1 inhibitory activities. Compounds **60b**,**c** exhibited much potent (60- to 100-fold) than that of **60a**,**d**. The substitution (Cl or Br) on 5-pyrinmidine of **60** has a little effect on the Akt1 inhibitory activities, and bromine is slightly better. Moreover, correlating predictive and experimental activities revealed that moderate linear relation coefficient was observed ($R^2 = 0.575$), indicating that the trend of them are the same. Except for **60a**, compounds **60b**–**c** with preferable predictive activities also showed better experimental activities than compounds **56a**,**b**. Especially for compounds **60b** and **60c**, the prediction results are very accurate that the derivation for them are −0.11 and 0.18, respectively.

The antiproliferative activities of compounds **56a**,**b** and **60a**–**d** against cancer cell lines (OVCAR-8 and HCT116) was investigated, since that Akt1 is an anti-apoptotic protein kinase and the blockade of its activity leads to cell death. As expected, compounds **60b** and **60c** showed good anti-proliferative activities against HCT116 (**60b**: $IC_{50} = 4.36$ μM; **60c**: $IC_{50} = 5.15$ μM) and more potent than that against OVCAR-8 (**60b**: $IC_{50} = 26.07$ μM; **60c**: $IC_{50} = 22.67$ μM) cell lines. In antiproliferative activities against HCT116, three compounds **60b**–**d** with preferable Akt1 inhibitory activities ($IC_{50} < 0.5$ μM) exhibited more potent antiproliferative activities (3- to 4-fold) than that of **56a**,**b** and **60a**.

## 4. Conclusion

In this study, we described an improved molecular docking based QSAR model for Akt1 inhibitors. The **MD-SVR** model was established using support vector regression (SVR) method. A combination of docking scores, key interaction profiles and molecular descriptors of the Akt1 inhibitors were considered in QSAR modeling. The **MD-SVR** model was extensively validated and showed good statistical parameters. Then, the application of **MD-SVR** model in optimization of 4-aminopyrimidine derivatives as novel Akt1 inhibitors was performed, and all of them exhibited moderate to good Akt1 inhibitory activities. It was demonstrated that the reliability and accuracy of the established **MD-SVR** model is promising, since that moderate linear relation coefficient was observed by correlating predictive and experimental activities. To the best of our knowledge, the integration of additional variables into molecular docking model for Akt1 inhibitors and its subsequent application in structure-based drug design was reported for the first time. Moreover, compound **60c**, the most potent one ($IC_{50} = 7.7$ nM), would be a good lead to do further structure-activity research to find high potent inhibitors.

## 5. Experimental

### 5.1. Chemistry

Melting points were obtained on a B-540 Büchi melting-point apparatus and are uncorrected. $^1$H NMR spectra were recorded on a 500 MHz, $^{13}$C NMR were recorded on a 125 or 100 MHz spectrometer (chemical shifts are given in ppm (d) relative to TMS as internal standard, coupling constants (*J*) are in hertz (Hz), and signals are designated as follows: s, singlet; d, doublet; t, triplet; m, multiplet; br s, broad singlet, etc.). Mass spectral data were obtained on an Esquire-LC-00075 spectrometer. High resolution mass spectra were measured on an Agilent 1290 HPLC-6224 Time of Fight Mass Spectrometer.

#### 5.1.1. N,N-Bis(2-hydroxyethyl)-N-benzylamine ***49***

To a stirred solution of diethanolamine **48** (21 g, 200 mmol) and anhydrous $K_2CO_3$ (55.2 g, 400 mmol) in dry acetonitrile (500 mL) was added dropwise benzyl bromide (34.2 g, 200 mmol). The mixture was stirred at 80 °C for 10 h, after cooling, the potassium salts were filtered off and the reaction mixture was concentrated. The residue was extracted with ethyl acetate and washed with water. The organic layer was further washed well with brine, dried over anhydrous $Na_2SO_4$, and then concentrated under vacuum to give the title compound (36.2 g, 93%) as a colorless oil, which was characterized by LC-MS (*m/z*: 196 $[M + 1]^+$) and then used directly in the next step without further purification.

#### 5.1.2. N,N-Bis(2-chloroethyl)benzylamine hydrochloride ***50***

To a solution of **49** (19.5 g, 0.1 mol) in dry $CH_2Cl_2$ (200 mL) at 0 °C was added $SOCl_2$ (60 mL) in one portion. The mixture was stirred at 25 °C for 2 h, then at 50 °C for 1 h. After cooling, ethyl ether (400 mL) was added, and then the precipitate was filtrated, rinsed with ethyl ether and dried to afford the title compound (25 g, 94%) as a white solid, mp: 148–150 °C. $^1$H NMR (500 MHz, DMSO-$d_6$) $\delta$ 11.94 (s, 1H), 7.64 (s, 2H), 7.37 (d, $J = 15.4$ Hz, 3H), 4.42 (s, 2H), 4.02 (s, 4H), 3.39 (s, 4H). ESI-MS (*m/z*): 232 $[M + 1]^+$.

#### 5.1.3. 1-Benzyl-4-(3,4-dichlorophenyl)piperidine-4-carbonitrile ***51***

To a well stirred suspension of **50** (5.37 g, 20 mmol), 2-(3,4-dichlorophenyl)acetonitrile (4.1 g, 22 mmol) and tetrabutylammonium hydrogen sulfate (0.68 g, 2 mmol) in toluene (15 mL) was added dropwise 10 g of 50% (w/w) aqueous sodium hydroxide solution. The reaction mixture was heated at 85 °C for 4 h, then poured into ice-water (50 mL) and extracted with ethyl ether (25 mL × 3). The combined organic layers were dried over anhydrous $Na_2SO_4$, concentrated under vacuum. The residue was purified on silica gel to afford the title compound (4.3 g, 63%) as a yellow oil. $^1$H NMR (500 MHz, $CDCl_3$) $\delta$ 7.59 (d, $J = 2.3$ Hz, 1H), 7.48–7.46 (m, 1H), 7.37–7.32 (m, 5H), 7.31–7.26 (m, 1H), 3.60 (s, 2H), 3.01 (d, $J = 12.5$ Hz, 2H), 2.56–2.42 (m, 2H), 2.09–2.05 (m, 4H). ESI-MS (*m/z*): 345 $[M + 1]^+$.

#### 5.1.4. 4-(3,4-Dichlorophenyl)piperidine-4-carbonitrile hydrochloride salt ***52***

To a solution of **51** (3.1 g, 9 mmol) in 1,2-dichloroethane (50 mL) was added 2-chloroethyl chloroformate (1.5 g, 11 mmol), and the mixture was heated to 100 °C for 2 h. The mixture was cooled to 25 °C and concentrated under reduced pressure. The crude residue was dissolved in MeOH (50 mL) and heated to reflux for 3 h. The mixture was cooled to room temperature, and concentrated under reduced pressure to yield the title compound (2.35 g, 90%), as a white solid, mp: > 250 °C. $^1$H NMR (500 MHz, DMSO-$d_6$) $\delta$ 9.58 (s, 1H), 9.38 (s, 1H), 7.80–7.76 (m, 2H), 7.55 (dd, $J = 8.5$, 2.4 Hz, 1H),

3.48 (d, $J$ = 13.5 Hz, 2H), 3.12–3.00 (m, 2H), 2.47–2.41 (m, 4H). ESI-MS ($m/z$): 255 $[M + 1]^+$.

*5.1.5. General procedure for preparation of compound **54***

To a suspension of 4,6-dichloropyrimidine **53** (3.0 g, 20 mmol) in isopropanol (40 mL) was added appropriate amine at such a rate that the internal temperature did not rise above 40 °C. After completion of the addition, the reaction mixture was stirred for 1 h at 25 °C. Water (30 mL) was added, and the resulting suspension was cooled in an ice bath to 0 °C. The precipitated product was filtered off and washed with cold isopropanol/water (2:1, 50 mL) and water. The collected material was dried in vacuo to afford the title compounds.

*5.1.5.1. 6-Chloro-N-methylpyrimidin-4-amine **54a**.* Reagent: 33% methylamine in ethanol (20 mL, 165 mmol). The product was obtained as a white solid (2.6 g, 91%), mp: 137–139 °C. $^1$H NMR (500 MHz, DMSO-$d_6$) $\delta$ 8.23 (s, 1H), 7.67 (s, 1H), 6.49 (d, $J$ = 0.8 Hz, 1H), 2.77 (d, $J$ = 0.8 Hz, 3H). ESI-MS ($m/z$): 144 $[M + 1]^+$.

*5.1.5.2. 6-Chloropyrimidin-4-amine **54b**.* Reagent: ammonia solution (10 mL, 165 mmol). The product was obtained as a white solid (2.6 g, 88%), mp: 205–207 °C. $^1$H NMR (500 MHz, DMSO-$d_6$) $\delta$ 8.19 (s, 1H), 7.22 (s, 2H), 6.43 (s, 1H). ESI-MS ($m/z$): 130 $[M + 1]^+$.

*5.1.6. General procedure for preparation of compound **55***

To a solution of **5**2(290 mg, 1 mmol) in DMF (15 mL) was added **54** and $K_2CO_3$ (414 mg, 3 mmol) and the reaction mixture was heat to 100 °C in a sealed tube for 5 h. Then, the reaction solution was poured into water (30 mL) and extracted with ethyl acetate (25 mL × 3). The combined organic layers were dried over $Na_2SO_4$, concentrated under vacuum and purified on silica gel to afford the title compounds.

*5.1.6.1. 4-(3,4-Dichlorophenyl)-1-(6-(methylamino)pyrimidin-4-yl) piperidine-4-carbonitrile **55a**.* Reagent: **54a** (172 mg, 1.2 mmol). The product was obtained as a white solid (188 mg, 52%), mp: 181–183 °C. $^1$H NMR (500 MHz, $CDCl_3$) $\delta$ 8.19 (s, 1H), 7.58 (d, $J$ = 2.3 Hz, 1H), 7.51 (d, $J$ = 8.5 Hz, 1H), 7.35 (dd, $J$ = 8.5, 2.3 Hz, 1H), 5.48 (s, 1H), 4.95 (s, 1H), 4.57 (d, $J$ = 14.0 Hz, 2H), 3.36–3.29 (m, 2H), 2.92 (d, $J$ = 5.2 Hz, 3H), 2.19 (d, $J$ = 11.6 Hz, 2H), 2.00 (td, $J$ = 13.2, 4.1 Hz, 2H). ESI-MS ($m/z$): 362 $[M + 1]^+$.

*5.1.6.2. 1-(6-Aminopyrimidin-4-yl)-4-(3,4-dichlorophenyl)piperidine-4-carbonitrile **55b**.* Reagent: **54a** (155 mg, 1.2 mmol). The product was obtained as a white solid (167 mg, 48%), mp: 195–198 °C. $^1$H NMR (500 MHz, $CDCl_3$) $\delta$ 8.23 (s, $J$ = 0.7 Hz, 1H), 7.57 (d, $J$ = 2.3 Hz, 1H), 7.50 (dd, $J$ = 11.0, 6.7 Hz, 1H), 7.34 (dd, $J$ = 8.5, 2.4 Hz, 1H), 5.67 (d, $J$ = 0.8 Hz, 1H), 4.70 (s, 2H), 4.53 (d, $J$ = 13.9 Hz, 2H), 3.35–3.28 (m, 2H), 2.21–2.15 (m, 2H), 1.99 (td, $J$ = 13.4, 4.2 Hz, 2H). ESI-MS ($m/z$): 348 $[M + 1]^+$.

*5.1.7. General procedure for preparation of compound **56***

A suspension of $AlCl_3$ (66.5 mg, 0.5 mmol) in dry THF (10 mL) was added to a suspension of $LiAlH_4$ (20 mg, 0.53 mmol) in THF (10 mL) at 0 °C and this mixture was stirred for 10 min followed by the dropwise addition of a solution of **55** in THF (5 mL). The reaction mixture was allowed to warm to room temperature, stirred overnight, cooled with an ice bath, and quenched with a saturated solution of $Na_2CO_3$ in water until the foaming stopped. Subsequently, the suspension was filtered, and the filtrate was dried over $Na_2SO_4$, concentrated under vacuum and purified on silica gel to afford the title compounds.

*5.1.7.1. 6-(4-(Aminomethyl)-4-(3,4-dichlorophenyl)piperidin-1-yl)-N-methylpyrimidin-4-amine **56a**.* Reagent: **55a** (90 mg, 0.25 mmol). The product was obtained as a white solid (61 mg, 67%), mp: 128–130 °C. 1H NMR (500 MHz, DMSO-$d_6$) $\delta$ 8.02 (s, 1H), 7.82 (d, $J$ = 2.2 Hz, 1H), 7.71 (d, $J$ = 8.5 Hz, 1H), 7.57 (dd, $J$ = 8.5, 2.3 Hz, 1H), 6.67 (d, $J$ = 4.7 Hz, 1H), 5.66 (s, 1H), 4.49 (s, 2H), 3.30 (d, $J$ = 11.7 Hz, 1H), 3.04 (t, $J$ = 12.3 Hz, 2H), 2.74 (d, $J$ = 4.6 Hz, 3H), 2.23 (d, $J$ = 12.8 Hz, 2H), 2.00 (td, $J$ = 13.1, 3.8 Hz, 2H). $^{13}$C NMR (125 MHz, DMSO-$d_6$) $\delta$ 164.5, 164.4, 162.2, 157.7, 141.2, 132.3, 131.6, 131.5, 128.6, 126.9, 121.6, 42.7, 41.8, 34.8, 28.1. ESI-MS ($m/z$): 366 $[M + 1]^+$. HRMS (ESI): $m/z$ calcd for $(C_{17}H_{21}Cl_2N_5+H)^+$: 366.1252; found: 366.1255.

*5.1.7.2. 6-(4-(Aminomethyl)-4-(3,4-dichlorophenyl)piperidin-1-yl) pyrimidin-4-amine **56b**.* Reagent: **55a** (87 mg, 0.25 mmol) The product was obtained as a white solid (55 mg, 62%), mp: 146–148 °C. $^1$H NMR (500 MHz, $CDCl_3$) $\delta$ 8.18 (s, 1H), 7.47 (d, $J$ = 8.5 Hz, 1H), 7.43 (d, $J$ = 2.2 Hz, 1H), 7.20 (dd, $J$ = 8.5, 2.3 Hz, 1H), 5.58 (s, 1H), 4.52 (s, 2H), 3.88 (dt, $J$ = 10.7, 5.4 Hz, 2H), 3.22 (ddd, $J$ = 13.2, 10.0, 3.0 Hz, 2H), 2.82 (s, 2H), 2.19 (d, $J$ = 14.2 Hz, 2H), 1.83 (ddd, $J$ = 13.9, 10.0, 3.9 Hz, 2H). ESI-MS ($m/z$): 352 $[M+1]^+$. HRMS (ESI): $m/z$ calcd for $(C_{16}H_{19}Cl_2N_5+H)^+$: 352.1096; found: 352.1200.

*5.1.8. Tert-butyl 4-(6-aminopyrimidin-4-yl)piperazine-1-carboxylate **57***

A solution of **54b** (1.3 g, 10 mmol), N-Boc-piperazine (2.0 g, 11 mmol), and N,N-diisopropylethylamine (3.9 g, 30 mmol) in n-BuOH (50 mL) was heated to refluxing under a nitrogen atmosphere for 10 h. The reaction mixture was concentrated under vacuum, and the crude residue was purified by silica gel chromatography to afford the title compound (2.15 g, 77%) as a white solid, mp: 187–189 °C. $^1$H NMR (500 MHz, $CDCl_3$) $\delta$ 8.18 (s, 1H), 5.56 (s, 1H), 4.66 (s, 2H), 3.54 (s, 4H), 3.50 (s, 4H), 1.48 (s, 9H). ESI-MS ($m/z$): 280 $[M + 1]^+$.

*5.1.9. General procedure for preparation of compound **58***

A mixture of **57** (1.4 g, 5 mmol) and NCS or NBS in dry THF (30 mL) was stirred at 50 °C for 5 h. The reaction mixture was concentrated and the crude residue was recrystallized from ethyl acetate to give the title compound.

*5.1.9.1. Tert-butyl 4-(6-amino-5-chloropyrimidin-4-yl)piperazine-1-carboxylate **58a**.* Reagent: NCS (0.8 g, 6 mmol). The product was obtained as a white solid (1.3 g, 81%), mp: 149–151 °C. $^1$H NMR (500 MHz, $CDCl_3$) $\delta$ 8.10 (s, 1H), 5.28 (s, 2H), 3.53 (s, 8H), 1.47 (s, 9H). ESI-MS ($m/z$): 314 $[M + 1]^+$.

*5.1.9.2. Tert-butyl 4-(6-amino-5-bromopyrimidin-4-yl)piperazine-1-carboxylate **58b**.* Reagent: NBS (1.1 g, 6 mmol). The product was obtained as white solid (1.55 g, 87%), mp: 172–174 °C. $^1$H NMR (500 MHz, $CDCl_3$) $\delta$ 8.13 (s, 1H), 5.35 (s, 2H), 3.57–3.44 (m, 8H), 1.48 (s, 9H). ESI-MS ($m/z$): 358 $[M + 1]^+$.

*5.1.10. General procedure for preparation of compound **59***

To a solution of **58** in $CH_2Cl_2$ (15 mL) was added trifluoroacetic acid (3 mL) under ice-cooling. The reaction mixture was stirred at 25 °C for 3 h and concentrated in vacuo. The residue was treated with 1 N aqueous solution of NaOH and extracted with $CH_2Cl_2$. The extract was dried over anhydrous $Na_2SO_4$ and concentrated in vacuo to give the title compound.

*5.1.10.1. 5-Chloro-6-(piperazin-1-yl)pyrimidin-4-amine **59a**.* Reagent: **58a** (1.56 g, 5 mmol). The product was obtained as pale yellow powder (1.0 g, 95%), mp: 167–169 °C. $^1$H NMR (500 MHz, DMSO-$d_6$) $\delta$ 7.96 (s, 1H), 6.80 (s, 2H), 3.36–3.31 (m, 4H), 2.83–2.79 (m, 4H). ESI-MS ($m/z$): 214 $[M + 1]^+$.

*5.1.10.2. 5-Bromo-6-(piperazin-1-yl)pyrimidin-4-amine* ***59b***. Reagent: **58b** (1.79 g, 5 mmol). The product was obtained as a white solid (1.25, 97%), mp: 163–165 °C. $^1$H NMR (500 MHz, $CDCl_3$) $\delta$ 8.13 (s, 1H), 5.23 (s, 2H), 3.49–3.45 (m, 4H), 3.00–2.97 (m, 4H). ESI-MS (*m/z*): 258 $[M + 1]^+$.

*5.1.11. General procedure for synthesis of compound* ***60***

A mixture of N-Boc-phenylalanine, 1-hydroxybenzotriazole (91 mg, 0.6 mmol), 1-ethyl-3-(3-dimethyllaminopropyl)carbodiimide hydrochloride (115 mg, 0.6 mmol) and N,N-diisopropylethylamine (129 mg, 1 mmol) in dry $CH_2Cl_2$ (10 mL) at 0 °C was added compound **59**. After stirring for 15 min, the cold bath was removed, and the reaction mixture was stirred at 25 °C overnight and concentrated in vacuo. The resulting residue was added $H_2O$ (10 mL) and extracted with EtOAc, the combined organic layers were dried over $Na_2SO_4$, concentrated to afford a white solid. To a solution of the above solid in $CH_2Cl_2$ (7 mL) was added trifluoroacetic acid (1 mL) under ice-cooling. The reaction mixture was stirred at 25 °C for 2 h and concentrated in vacuo. The residue was treated with 1 N aqueous solution of NaOH and extracted with $CH_2Cl_2$. The extract was dried over anhydrous $Na_2SO_4$ and purified on silica gel to afford the title compound.

*5.1.11.1. (S)-2-Amino-1-(4-(6-amino-5-chloropyrimidin-4-yl)piperazin-1-yl)-3-phenylpropan-1-one* ***60a***. Reagent: *(S)*-2-((tert-butoxycarbonyl)amino)-3-phenylpropanoic acid (132 mg, 0.5 mmol) and **59a** (106.7 mg, 0.5 mmol). The product was obtained as a white solid (95 mg, 53%), mp: 129–132 °C. $^1$H NMR (500 MHz, $CDCl_3$) $\delta$ 8.04 (s, 1H), 7.32–7.26 (m, 2H), 7.24–7.16 (m, 3H), 5.49 (s, 2H), 4.10 (t, $J$ = 7.2 Hz, 1H), 3.74–3.67 (m, 1H), 3.64–3.55 (m, 1H), 3.54–3.43 (m, 2H), 3.42–3.34 (m, 2H), 3.34–3.27 (m, 1H), 2.99–2.89 (m, 2H), 2.89–2.81 (m, 1H). $^{13}$C NMR (125 MHz, $CDCl_3$) $\delta$ 172.9, 160.5, 160.5, 154.4, 136.7, 129.4, 128.8, 127.2, 98.0, 52.2, 47.3, 47.1, 45.6, 45.1, 42.0. ESI-MS (*m/z*): 361 $[M + 1]^+$. HRMS (ESI): *m/z* calcd for $(C_{17}H_{21}ClN_6O + H)^+$: 361.1544; found: 361.1539.

*5.1.11.2. (±)-2-Amino-1-(4-(6-amino-5-chloropyrimidin-4-yl)piperazin-1-yl)-3-(4-chlorophenyl) propan-1-one* ***60b***. Reagent: 2-((tert-butoxycarbonyl)amino)-3-(4-chlorophenyl)propanoic acid (150 mg, 0.5 mmol) and **59a** (106.7 mg, 0.5 mmol). The product was obtained as a white solid (92.8 mg, 47%), mp: 151–153 °C. $^1$H NMR (500 MHz, $CDCl_3$) $\delta$ 8.09 (s, 1H), 7.28–7.26 (m, 2H), 7.15–7.12 (m, 2H), 5.30 (s, 2H), 3.96–3.88 (m, 1H), 3.74–3.64 (m, 2H), 3.56–3.37 (m, 4H), 3.30–3.09 (m, 2H), 2.97–2.88 (m, 1H), 2.78 (dd, $J$ = 13.4, 7.2 Hz, 1H). $^{13}$C NMR (125 MHz, $CDCl_3$) $\delta$ 173.2, 160.7, 160.4, 154.6, 136.0, 132.8, 130.7, 128.8, 98.3, 52.4, 47.7, 47.5, 45.1, 42.1, 41.9. ESI-MS (*m/z*): 395 $[M + 1]^+$. HRMS (ESI): *m/z* calcd for $(C_{17}H_{20}Cl_2N_6O + H)^+$: 395.1154; found: 395.1158.

*5.1.11.3. (±)-2-Amino-1-(4-(6-amino-5-bromopyrimidin-4-yl)piperazin-1-yl)-3-(4-chlorophenyl) propan-1-one* ***60c***. Reagent: 2-((Tert-butoxycarbonyl)amino)-3-(4-chlorophenyl)propanoic acid (150 mg, 0.5 mmol) and **59b** (129 mg, 0.5 mmol). The product was obtained as a white solid (138.5 mg, 63%), mp: 166–168 °C. $^1$H NMR (500 MHz, $CDCl_3$) $\delta$ 8.13 (s, 1H), 7.28 (d, $J$ = 8.3 Hz, 2H), 7.15 (d, $J$ = 8.3 Hz, 2H), 5.27 (s, 2H), 3.93 (t, $J$ = 7.1 Hz, 1H), 3.72 (t, $J$ = 5.1 Hz, 2H), 3.56–3.44 (m, 2H), 3.43–3.35 (m, 2H), 3.31–3.26 (m, 1H), 3.15–3.07 (m, 1H), 2.94 (dd, $J$ = 13.4, 6.9 Hz, 1H), 2.79 (dd, $J$ = 13.4, 7.2 Hz, 1H). $^{13}$C NMR (125 MHz, $CDCl_3$) $\delta$ 173.3, 162.9, 161.5, 155.5, 136.0, 132.8, 130.7, 128.8, 89.3, 52.4, 48.3, 48.1, 45.1, 42.1, 41.9. ESI-MS (*m/z*): 439 $[M + 1]^+$. HRMS (ESI): *m/z* calcd for $(C_{17}H_{20}BrClN_6O + H)^+$: 439.0649; found: 439.0652.

*5.1.11.4. (±)-2-Amino-1-(4-(6-amino-5-bromopyrimidin-4-yl)piperazin-1-yl)-3-phenylpropan-1-one* ***60d***. Reagent: *(S)*-2-((tert-butoxycarbonyl)amino)-3-phenylpropanoic acid (132 mg, 0.5 mmol) and **59b** (129 mg, 0.5 mmol). The product was obtained as a white solid (119 mg, 59%), mp: 143–145 °C. $^1$H NMR (500 MHz, $CDCl_3$) $\delta$ 8.08 (s, 1H), 7.32–7.27 (m, 2H), 7.24–7.17 (m, 3H), 5.50 (s, 2H), 3.97 (t, $J$ = 7.2 Hz, 1H), 3.75 (m, 1H), 3.60 (m, 1H), 3.51–3.40 (m, 2H), 3.39–3.31 (m, 1H), 3.32–3.24 (m, 1H), 3.23–3.15 (m, 1H), 2.98–2.90 (m, 1H), 2.88–2.81 (m, 2H). $^{13}$C NMR (125 MHz, $CDCl_3$) $\delta$ 173.4, 162.8, 161.5, 155.4, 137.4, 129.4, 128.7, 127.0, 89.0, 52.5, 48.2, 47.9, 45.0, 43.0, 41.8. ESI-MS (*m/z*): 405 $[M + 1]^+$. HRMS (ESI): *m/z* calcd for $(C_{17}H_{21}BrN_6O + H)^+$: 405.1038; found: 405.1040.

*5.2. Pharmacological assay*

*5.2.1. Akt1 assay*

AKT1/PKBα Kinase Assay Kit (catalog No. 32-021) and active recombinant AKT1 kinase were commercially available from UPSTATE (acquired by Merck Millipore, Billerica, MA). 4 ng of Akt1 in 8 μL of 2.5 × kinase buffer [62.5 mM Tris–HCl (pH 7.5), 25 mM $MgCl_2$, 12.5 mM β-glycerophosphate, 0.25 mM $Na_3VO4$, 5 mM dithiothreitol (DTT)], was mixed with 2 μL of dimethyl sulfoxide (DMSO) vehicle or each of the compound (indicated concentrations), incubated at room temperature for 5 min and 10 μL of ATP/substrate cocktail (20 mM ATP, 3 mM eNOS served as substrate) was added. After incubation at room temperature for 30 min, add 20 μL of 50 mM ethylenediaminetetraacetic acid (EDTA) (pH 8.0) and terminate the reaction. Then, PKB/Akt1 kinase activity was analyzed according to the manufacturer's instructions.

*5.2.2. Cytotoxic activity assay.* The cytotoxic activity of the tested compounds in OVCAR-8 and HCT116 cells was measured using the MTT (3-(4,5-Dimethylthiazol-2-yl)-2,5-diphenyltetrazolium bromide, a tetrazole) method. Cells were seeded in 96-well microtiter plates (at a density of 4000 cells per well) for overnight attachment and exposed to each of the test compound (1.0–100.0 μM) for 72 h. The MTT solution (5.0 mg/mL in RPIM 1640 medium; Sigma–Aldrich) was added (20.0 μl/well), and plates were incubated for a further 4 h at 37 °C. The purple formazan crystals were dissolved in 100.0 μL of DMSO. After 5 min, the plates were read on an automated microplate spectrophotometer (Bio-Tek Instruments, Winooski, VT) at 570 nm. Assays were performed in triplicate on three independent experiments. The concentration of drug inhibiting 50% of cells ($IC_{50}$) was calculated using the software of dose-effect analysis.

## Acknowledgment

We thank Mrs. Jianyang Pan (Pharmaceutical Informatics Institute, Zhejiang University) for performing the NMR spectrometry. This study was financially supported by National Natural Science Foundation of China (No. 81001359), Medical Scientific Research Foundation of Zhejiang Province (NO. 2010KYA061), Zhejiang Provincial Natural Science Foundation of China (LY13H300002) and Program for Zhejiang Leading Team of S&T Innovation.

## Appendix A. Supplementary data

Supplementary data related to this article can be found at http://dx.doi.org/10.1016/j.ejmech.2014.01.019.

## References

[1] V. Vapnik, C. Cortes, Support vector networks, Mach. Learn. 20 (1995) 273–297.
[2] J. Levatic, J. Curak, M. Kralj, T. Smuc, M. Osmak, F. Supek, Accurate models for P-gp drug recognition induced from a cancer cell line cytotoxicity screen, J. Med. Chem. 56 (2013) 5691–5708.

[3] R. Varela, W.P. Walters, B.B. Goldman, A.N. Jain, Iterative refinement of a binding pocket model: active computational steering of lead optimization, J. Med. Chem. 55 (2012) 8926–8942.
[4] W. Wang, W. He, X. Zhou, X. Chen, Optimization of molecular docking scores with support vector rank regression, Proteins 81 (2013) 1386–1398.
[5] P.J. Ballester, J.B. Mitchell, A machine learning approach to predicting protein–ligand binding affinity with applications to molecular docking, Bioinformatics 26 (2010) 1169–1175.
[6] S. Li, L. Xi, C. Wang, J. Li, B. Lei, H. Liu, X. Yao, A novel method for protein–ligand binding affinity prediction and the related descriptors exploration, J. Comput. Chem. 30 (2009) 900–909.
[7] S. Das, M.P. Krein, C.M. Breneman, Binding affinity prediction with property-encoded shape distribution signatures, J. Chem. Inf. Model. 50 (2010) 298–308.
[8] S.P. Staal, Molecular cloning of the akt oncogene and its human homologues AKT1 and AKT2: amplification of AKT1 in a primary human gastric adenocarcinoma, Proc. Natl. Acad. Sci. U. S. A. 84 (1987) 5034–5037.
[9] J.Q. Cheng, B. Ruggeri, W.M. Klein, G. Sonoda, D.A. Altomare, D.K. Watson, J.R. Testa, Amplification of AKT2 in human pancreatic cancer cells and inhibition of AKT2 expression and tumorigenicity by antisense RNA, Proc. Natl. Acad. Sci. U. S. A. 93 (1996) 3636–3641.
[10] J.Q. Cheng, C.W. Lindsley, G.Z. Cheng, H. Yang, S.V. Nicosia, The Akt/PKB pathway: molecular target for cancer drug discovery, Oncogene 24 (2005) 7482–7492.
[11] R.T. Joseph, B. Alfonso, AKT plays a central role in tumorigenesis, Proc. Natl. Acad. Sci. U. S. A. 98 (2001) 10983–10985.
[12] L.C. Cantley, The phosphoinositide 3-kinase pathway, Science 296 (2002) 1655–1657.
[13] B.D. Manning, L.C. Cantley, AKT/PKB signaling: navigating downstream, Cell 129 (2007) 1261–1274.
[14] L. Salmena, A. Carracedo, P.P. Pandolfi, Tenets of PTEN tumor suppression, Cell 133 (2008) 403–414.
[15] A. Carnero, C. Blanco-Aparicio, O. Renner, W. Link, J.F. Leal, The PTEN/PI3K/AKT signalling pathway in cancer, therapeutic implications, Curr. Cancer Drug Targets 8 (2008) 187–198.
[16] M. Addie, P. Ballard, D. Buttar, C. Crafter, G. Currie, B.R. Davies, J. Debreczeni, H. Dry, P. Dudley, R. Greenwood, P.D. Johnson, J.G. Kettle, C. Lane, G. Lamont, A. Leach, R.W. Luke, J. Morris, D. Ogilvie, K. Page, M. Pass, S. Pearson, L. Ruston, Discovery of 4-amino-N-[(1S)-1-(4-chlorophenyl)-3-hydroxypropyl]-1-(7H-pyrrolo[2,3-d]pyrimidin -4-yl)piperidine-4-carboxamide (AZD5363), an orally bioavailable, potent inhibitor of Akt kinases, J. Med. Chem. 56 (2013) 2059–2073.
[17] M.A. Ashwell, J.M. Lapierre, C. Brassard, K. Bresciano, C. Bull, S. Cornell-Kennon, S. Eathiraj, D.S. France, T. Hall, J. Hill, E. Kelleher, S. Khanapurkar, D. Kizer, S. Koerner, J. Link, Y. Liu, S. Makhija, M. Moussa, N. Namdev, K. Nguyen, R. Nicewonger, R. Palma, J. Szwaya, M. Tandon, U. Uppalapati, D. Vensel, L.P. Volak, E. Volckova, N. Westlund, H. Wu, R.Y. Yang, T.C. Chan, Discovery and optimization of a series of 3-(3-phenyl-3H-imidazo[4,5-b]pyridin-2-yl) pyridin-2-amines: orally bioavailable, selective, and potent ATP-independent Akt inhibitors, J. Med. Chem. 55 (2012) 5291–5310.
[18] J.F. Blake, R. Xu, J.R. Bencsik, D. Xiao, N.C. Kallan, S. Schlachter, I.S. Mitchell, K.L. Spencer, A.L. Banka, E.M. Wallace, S.L. Gloor, M. Martinson, R.D. Woessner, G.P. Vigers, B.J. Brandhuber, J. Liang, B.S. Safina, J. Li, B. Zhang, C. Chabot, S. Do, L. Lee, J. Oeh, D. Sampath, B.B. Lee, K. Lin, B.M. Liederer, N.J. Skelton, Discovery and preclinical pharmacology of a selective ATP-competitive Akt inhibitor (GDC-0068) for the treatment of human tumors, J. Med. Chem. 55 (2012) 8110–8127.
[19] W.R. Chao, D. Yean, K. Amin, C. Green, L. Jong, Computer-aided rational drug design: a novel agent (SR13668) designed to mimic the unique anticancer mechanisms of dietary indole-3-carbinol to block Akt signaling, J. Med. Chem. 50 (2007) 3412–3415.
[20] J.G. Kettle, S. Brown, C. Crafter, B.R. Davies, P. Dudley, G. Fairley, P. Faulder, S. Fillery, H. Greenwood, J. Hawkins, M. James, K. Johnson, C.D. Lane, M. Pass, J.H. Pink, H. Plant, S.C. Cosulich, Diverse heterocyclic scaffolds as allosteric inhibitors of AKT, J. Med. Chem. 55 (2012) 1261–1273.
[21] S.B. Kondapaka, S.S. Singh, G.P. Dasmahapatra, E.A. Sausville, K.K. Roy, Perifosine, a novel alkylphospholipid, inhibits protein kinase B activation, Mol. Cancer Ther. 2 (2003) 1093–1103.
[22] X. Dong, C. Jiang, H. Hu, J. Yan, J. Chen, Y. Hu, QSAR study of Akt/protein kinase B (PKB) inhibitors using support vector machine, Eur. J. Med. Chem. 44 (2009) 4090–4097.
[23] X. Dong, X. Zhou, H. Jing, J. Chen, T. Liu, B. Yang, Q. He, Y. Hu, Pharmacophore identification, virtual screening and biological evaluation of prenylated flavonoids derivatives as PKB/Akt1 inhibitors, Eur. J. Med. Chem. 46 (2011) 5949–5958.
[24] M.A. Seefeld, M.B. Rouse, K.C. McNulty, L. Sun, J. Wang, D.S. Yamashita, J.I. Luengo, S. Zhang, E.A. Minthorn, N.O. Concha, D.A. Heerding, Discovery of 5-pyrrolopyridinyl-2-thiophenecarboxamides as potent AKT kinase inhibitors, Bioorg. Med. Chem. Lett. 19 (2009) 2244–2248.
[25] K.D. Freeman-Cook, C. Autry, G. Borzillo, D. Gordon, E. Barbacci-Tobin, V. Bernardo, D. Briere, T. Clark, M. Corbett, J. Jakubczak, S. Kakar, E. Knauth, B. Lippa, M.J. Luzzio, M. Mansour, G. Martinelli, M. Marx, K. Nelson, J. Pandit, F. Rajamohan, S. Robinson, C. Subramanyam, L. Wei, M. Wythes, J. Morris, Design of selective, ATP-competitive inhibitors of Akt, J. Med. Chem. 53 (2010) 4615–4622.
[26] B. Lippa, G. Pan, M. Corbett, C. Li, G.S. Kauffman, J. Pandit, S. Robinson, L. Wei, E. Kozina, E.S. Marr, G. Borzillo, E. Knauth, E.G. Barbacci-Tobin, P. Vincent, M. Troutman, D. Baker, F. Rajamohan, S. Kakar, T. Clark, J. Morris, Synthesis and structure based optimization of novel Akt inhibitors, Bioorg. Med. Chem. Lett. 18 (2008) 3359–3363.
[27] S. Chang, Z. Zhang, X. Zhuang, J. Luo, X. Cao, H. Li, Z. Tu, X. Lu, X. Ren, K. Ding, New thiazole carboxamides as potent inhibitors of Akt kinases, Bioorg Med. Chem. Lett. 22 (2012) 1208–1212.
[28] B.R. Brooks, R.E. Brucolleri, B.D. Olafson, D.J. States, S. Swaminathan, M. Karplus, CHARMM: a program for macromolecular energy, minimization, and dynamics calculations, J. Comput. Chem. 4 (1983) 187–214.
[29] C.M. Venkatachalam, X. Jiang, T. Oldfield, M. Waldman, LigandFit: a novel method for the shape-directed rapid docking of ligands to protein active sites, J. Mol. Graphics Modell. 21 (2003) 289–307.
[30] M. Montes, M.A. Miteva, B.O. Villoutreix, Structure-based virtual ligand screening with LigandFit: pose prediction and enrichment of compound collections, Proteins 68 (2007) 712–725.
[31] C.C. Kumar, V. Madison, Akt crystal structure and Akt-specific inhibitors, Oncogene 24 (2005) 7493–7501.